*Proceedings of the 21st ICSMGE, Vienna, Austria, 14 – 19 June 2026. Pistrol, Adam & Schweiger (eds.)*
*Published by: ÖGG, Austrian Society for Geomechanics, Salzburg, Austria, ISBN 978-3-9503898-4-5*
*https://doi.org/10.53243/ICSMGE2026-653*

# Air-Entry Value in Unsaturated Soils: Implications for Geotechnical Design

**Bestun J. Shwan**
*Water Resources Engineering Department, College of Engineering, Salahaddin University, Erbil, Iraq,*
*bestun.shwan@su.edu.krd*

ABSTRACT: In addition to the stress state variables (normal stress and matric suction), the air entry value (*AEV*) is a significant parameter in the field of unsaturated soil mechanics. It is influenced by pore size, hydraulic hysteresis, and mechanical hysteresis. While its effect on water retention is well recognized, its impact on the mechanical characteristics for various geotechnical applications is still underrepresented. This study numerically examines the effect of *AEV* on strength across different geotechnical problems: bearing capacity, slope, retaining wall, and tunnel, using the upper bound theorem under various suction profiles. Numerical results were validated against experimental and analytical solutions. For the bearing capacity problem, the numerical results showed a 4.83-fold increase in the bearing capacity factor (Nγ) was obtained when *AEV* increased from 2.3 kPa to 6 kPa at a suction value of 5.58 kPa for a rigid strip footing placed at the surface. For a fully frictional retaining wall, a 1.47-fold increase in passive earth pressure was obtained when the *AEV* increased from 5 to 20 kPa at an angle of shearing resistance of 30°, with the water table located 2 m below the base of the wall. To put this in context, this was equivalent to a 4.4° increase in the angle of shearing resistance at *AEV* = 5 kPa. Other modeled slope and tunnel problems also showed a significant effect of the *AEV*. Analysis of the failure mechanisms for the studied cases revealed different patterns at various *AEV*s.

KEYWORDS: Suction, Air Entry Value, Bearing Capacity, Slope, Retaining Wall, Tunnel, Hysteresis.

## 1 INTRODUCTION

The position of the water retention curve (WRC) is influenced by various factors: such as water content, drying and wetting cycles, soil fabric, void ratio (density), load application, and mineral composition, Vanapalli et al. (1999) and Lu and Likos (2004). Drying and wetting cycles causes so-called hydraulic hysteresis. Hydraulic hysteresis is generally defined as a difference in the degree of saturation/water content ($w$) at the same suction during drying and wetting cycles. The array of suction and water content ($s$, $w$) in Fig. 1a is bounded between the minimum (wetting) and maximum (drying) $s$ values being reached previously. Moreover, hydraulic hysteresis has a significant effect on the effective stress, Nuth and Laloui (2008). On the other hand, void ratio, density and load application cause mechanical hysteresis. As the void ratio (e) decreases, $s$ values tend to increase, causing the WRC to shift toward higher $s$ levels, see Fig. 1b.

Air entry value (*AEV*) is one of the most significant parameters of the WRC. It is the minimum $s$ required for air to enter the water-filled pores of a soil. In other words, it is the point on the WRC where the slope begins to drop steeply, indicating the onset of desaturation (see Fig. 1a). It has a significant influence on the mechanical characterization of soil, Romero (1999). Generally, soil is considered saturated when $s \leq AEV$.

The hydraulic and mechanical phenomena influence both the shape and position of the WRC and consequently the position of the *AEV*, Romero (1999) and Shwan (2017), (2023a) and (2023b). A change of 1.1 kPa in *AEV*, attributed to the hydraulic hysteresis, was reported by Shwan (2015) for a fine sand within a suction range of 0-6 kPa at null loading as shown in Fig. 1a. Differences of approximately 3 and 10 kPa in *AEV*, also attributed to the hydraulic hysteresis, were reported by Kim et al. (2018) and Pham et al. (2003) for weathered granite and silt soil, respectively.

On the other hand, mechanical hysteresis can also cause a shift of the *AEV*. For example, during the drying path, a shift of approximately 60 and 70 kPa in *AEV*, corresponding to a change in isotropic stress from 0 to 50 kPa and to 100 kPa for low-plasticity clay was reported by Chiu et al. (2014). In addition, on the drying path for a compacted clay, Vanapalli et al. (1999) reported a shift in *AEV* position of about 40 kPa when the void ratio decreased from 0.58 to 0.52. Similar mechanical hysteresis, indicating the evolution of *AEV* due to mechanical effects, was also reported by Tarantino and Tombolato (2005) and Nuth and Laloui (2008).

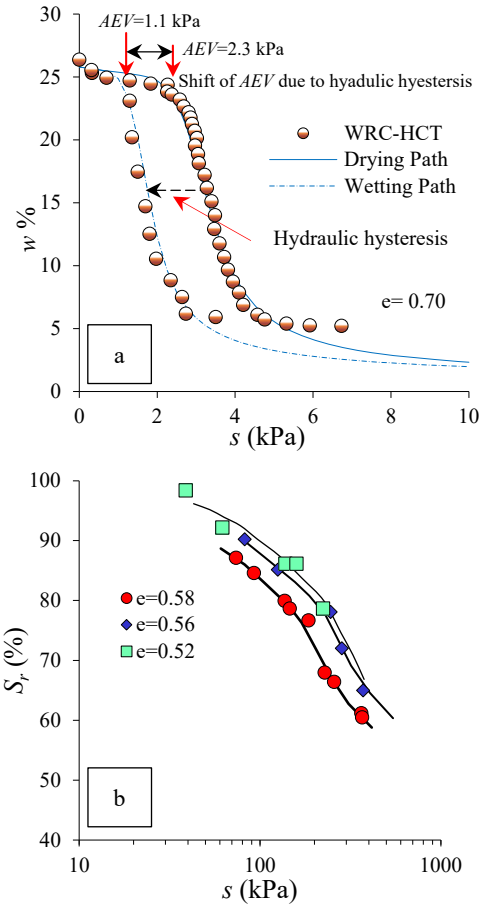


Figure 1. (a) Hydraulic hysteresis of the experimental WRC obtained using the hanging column technique (HCT), after Shwan (2015) and (b) Mechanical hysteresis due to void ratio changes, after Vanapalli et al (1999).

Although the change in *AEV* position due to hydraulic and mechanical hysteresis has been observed experimentally as stated above, its effect on the mechanical characterization of

various geotechnical problems, such as bearing capacity (**BC**), slopes (**SL**), retaining walls (**RW**), and tunnels (**TUN**), remains either entirely unstudied or only partly investigated. Attempts have been made; see for example, Shwan (2023b) who investigated the effect of changes in the shape of the SWRC on active earth pressure. This paper, therefore, extends the influence of *AEV* changes on the strength of various problems using a robust upper bound theorem approach, Discontinuity Layout Optimization for unsaturated soils (**UNSAT-DLO**). The approach was modified by the author to take into account the effects of unsaturated conditions on soil strength, see Shwan (2022), (2023c) and (2025).

## 2 MODELED PROBLEMS

The effect of *AEV* variations resulting from hydraulic (drying and wetting) and mechanical hysteresis was characterized for the different stated problems using the **UNSAT-DLO** approach under various suction profiles and drained conditions.

Table 1 summarizes the parameters used in the **UNSAT-DLO** approach for all problems, along with the range of *AEV*s modeled. The range of *AEV* variation depended on the soil type; the finer the soil, the greater the changes in *AEV*. Therefore, the modeled scenarios included different simulated soil types, ranging from sand to silty sand to capture a wide range of *AEV* variations.

The numerical case studies were validated against experimental results or analytical solutions. In the simulation, the soil above the water table height ($H_w$) was assumed to be fully saturated until the capillary rise height ($=AEV/\gamma_w$), where $\gamma_w$ is the unit weight of water. Above this zone, the soil was considered unsaturated until 1 m and beyond this threshold the soil was considered dry. In the numerical analysis, the soil was assumed to be fully saturated when $s \leq AEV$. This assumption was also utilized by others, e.g., Lloret-Cabot et al. (2018).

Table 1. Required parameters for the modeled problems.

| **Parameter** | **BC** | **SL** | **RW** | **TUN** |
|---|---|---|---|---|
| Saturated unit weight, $\gamma_{sat}$ (kN/m³) | 19.33 | 20 | 20 | 19.4 |
| Dry unit weight $\gamma_{dry}$ (kN/m³) | 15.13 | 15 | 15 | 15.4 |
| Unsaturated unit weight, $\gamma_{unsat}$ (kN/m³) | 17.32 | 17.5 | 17.5 | 17.4 |
| Cohesion, $c$ (kPa) | 0 | 0-25[1] | 0 | 0 |
| Angle of shearing resistance, $\phi$ (°) | 30-45[1] | 20-45[1] | 30 | 5-45[1] |
| Fitting parameter, κ (kPa$^{-1}$) | 0.7 | 0.05 | 0.05 | 0.01 |
| Air entry value, *AEV* (kPa) | 1-7[2] | 5-20[1] | 5-30[1] | 25-50[3] |
| Shotcrete strength, (kPa) | --- | --- | --- | 500 |

[1] increment 5 kPa, [2] increment 1 kPa, [3] increment 12.5 kPa.

### 2.1 *Bearing capacity (***BC***) problem.*

Figure 2a, b and c show the results of the **BC** problem at three different values of $s$ (2.158. 3.796 and 5.58 kPa). The problem consisted of modeling a rigid strip surface footing with a width of 25 mm on a bed of unsaturated fine sand. Suction was applied using the hanging column technique (HCT). The results were represented in terms of the bearing capacity factor ($N_\gamma$). $N_\gamma$ was obtained using the equation below:

$$N_\gamma = \frac{2Q_{ult}}{\gamma_d \times B} \qquad (1)$$

where $Q_{ult}$ is the ultimate bearing capacity (kPa), and $B$ is the width of the footing (m). The numerical analysis was validated against the experimental results conducted by Shwan (2015). The sand used had an *AEV* = 2.3 kPa on the drying path at null loading (no hysteresis). The markers in Fig. 2 represent the repeated tests at the same value of $s$, with an obvious scatter. Shwan (2023a) attributed this scatter to hydraulic and mechanical hysteresis effects.

In Fig. 2a, b, and c, the curves coincide when the applied $s \leq AEV$, consequently, no effect of *AEV* on **BC** and therefore on the obtained $N_\gamma$. This was attributed to the assumption that was made in the simulation, where soil was considered saturated when $s \leq AEV$ as stated previously. However, once the applied $s$ exceeded *AEV* (see Fig. 2b and c), the effect of *AEV* became evident on $N_\gamma$. The results of the modeled range of *AEV*s were in good agreement with the experimental results, suggesting that *AEV* has a significant influence on the bearing capacity. To further demonstrate this, an analytical study was carried out, as discussed below.

Figure 2d shows the change in $N_\gamma$ corresponding to changes in *AEV* for all three applied suction values. It can be seen that the effect of *AEV* on $N_\gamma$ is significant. For example, an increase of 1.49 in $N_\gamma$ was obtained when *AEV* increased from 1 kPa to 2.3 kPa for $s$ = 2.158 kPa at $\phi$ = 44°, see Fig. 2d. The changes were found even higher (1.88 and 4.83) for $s$ = 3.796 and 5.58 kPa when *AEV* increased from 2.3 kPa to 4 kPa and 6 kPa, respectively. To put this in context, this was equivalent to an increase of more than 3.5° in $\phi$ when modeling the case $s$ = 3.796 kPa at *AEV* = 2.3 kPa. On the other hand, a reduction in *AEV* to 1 kPa from 2.3 kPa at $s$ = 3.796 kPa, attributed to wetting, caused a decrease of more than 50% in BC (a decrease of 0.54 in $N_\gamma$).

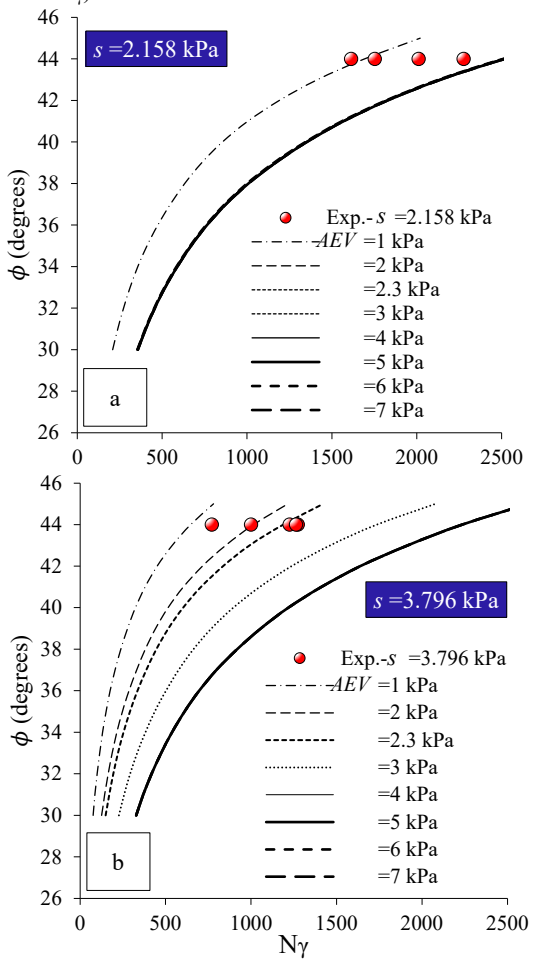

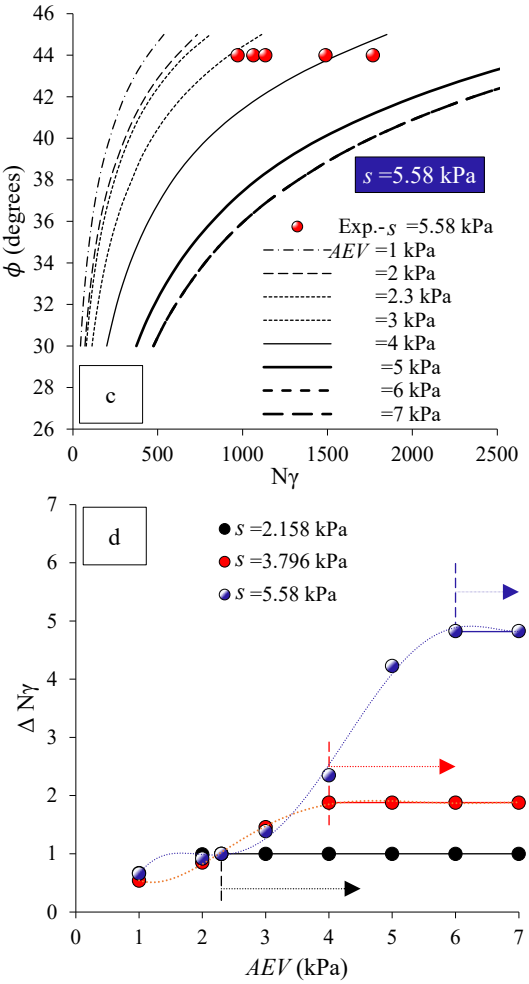


Figure 2. The effect of *AEV* on $N_\gamma$ for $s$ = (a) 2.158 kPa, (b) 3.796 kPa, (c) 5.58 kPa, and (d) the change in $N_\gamma$ for the three applied $s$.

The implication of the results presented in Fig. 2d is that hydraulic hysteresis (due to drying or wetting when *AEV* decreases) or mechanical hysteresis has a significant effect on $N_\gamma$.

In addition, the effect of *AEV* on failure modes was found to be significant. Figure 3 displays different failure modes (axisymmetric analysis) at various *AEV* values for $s$ = 5.58 kPa. The modeled cases were compared with the case of *AEV* = 2.3 kPa. The failure mechanism boundaries for *AEV* = 2.3 kPa were taken as a reference, i.e., the case not subjected to hydraulic or mechanical hysteresis. The red lines in Fig. 3 represent the failure mechanism boundaries for *AEV* = 2.3 kPa (which intersect the failure mechanism boundaries), drawn for comparison with other cases that deviate from these boundaries.

The analysis presented in Fig. 3 was performed with a scale factor (SF) of 700, instead of SF = 200 used in the results in Fig. 2a-d. The difference in the obtained bearing capacity for each *AEV* between SF = 200 and 700 is shown in Fig. 3. The SF in the **UNSAT-DLO** approach is defined as the number of spaces between the nodes per unit length. The higher SF was used to visualize the effect of even small changes in *AEV*.

Higher *AEV* (e.g., 6 kPa) resulted in deeper and wider failure mechanisms, exceeding the red lines of the reference case (*AEV* = 2.3 kPa), whereas lower *AEV* (e.g., 1 kPa) did not reach the boundaries of the reference. Higher *AEV* led to an increase in effective stress and frictional resistance, resulting in greater bearing capacity and, consequently, deeper and wider failure mechanisms.

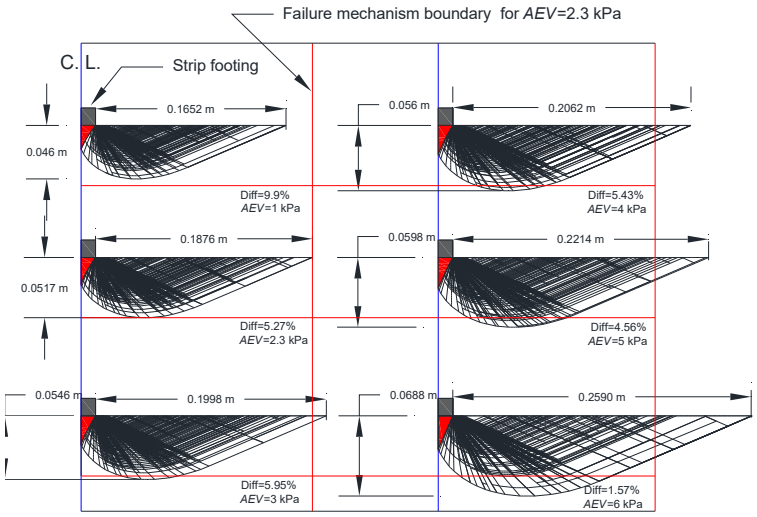


Figure 3. The effect of *AEV* on failure modes for the **BC** problem at different *AEV* values for $s$ = 5.58 kPa.

## 2.2 *Slope (**SL**) stability problem*

In this problem, a finite uniform slope with a height (H) of 1.5 m and slope inclination (β) of 45° was modeled at the water table height ($H_w$) = -3 m, 3 m below the origin (the origin was 1.5 m below the toe). $H_w$ = -3 m corresponds to a hydrostatic suction of 58.86 kPa, calculated as the distance from the water table to the surface of the slope. The results of the SL case study are presented as factor of safety (FS) and stability number (N). The stability number was first proposed by Bell (1966) and has been frequently used by others, e.g., Shwan (2023d).

A wider range of *AEV*s from 5 to 20 kPa was used in the simulations, representing a finer soil type, e.g., silty sand. The choice is based on the experimental findings as stated above, for example, Pham et al. (2003) reported a 10 kPa shift in *AEV* for silt soils due to hydraulic hysteresis, while Vanapalli et al. (1999) observed an even higher shift of 40 kPa due to mechanical hysteresis.

As in the case of the BC problem and as expected, it was found that the effect of *AEV* on FS was significant. The higher the *AEV*, the higher the stability and FS that was obtained. The overall trend showed an increase in FS with any increase in N (i.e., the shear strength parameter, c). An increase of 1.13 in FS was obtained when *AEV* increased from 5 to 20 kPa at c = 20 kPa and $\phi$ = 30°, which was equivalent to an increase of 10° in $\phi$ when modeling the case of *AEV* = 5 kPa at the same cohesion value.

Analysis of the failure mechanisms for the studied *AEV* values for the SL is shown in Fig. 5. Different failure modes for the modeled *AEV* values with FS displayed in each case were observed. Higher *AEV* resulted in wider failure mechanisms at the top (see the blue and yellow hatched slopes) with all cases showing the sliding surface intersecting the slope at the toe.

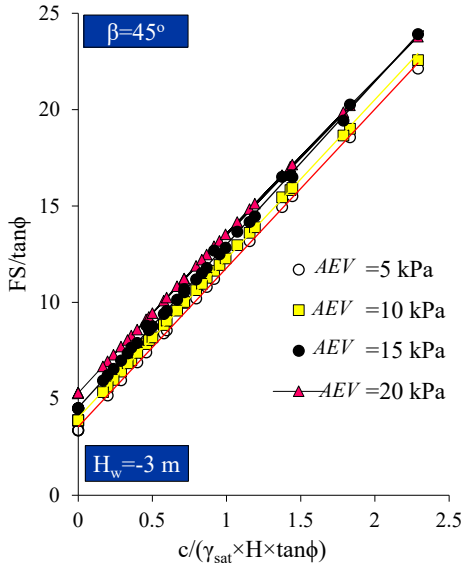


Figure 4. Normalized FS versus N results for various *AEV* values for the uniform slope (β = 45°) and $H_W$ = -3 m.

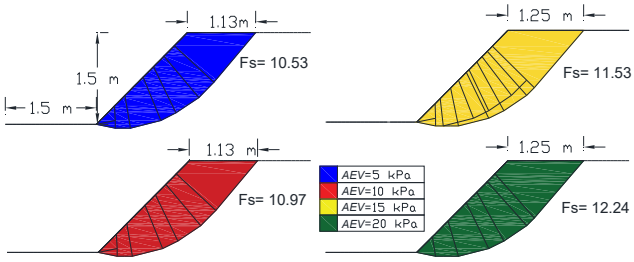


Figure 5. Failure modes for the **SL** problem at various *AEV* values for the uniform slope (β = 45°) and $H_W$ = -3 m.

### 2.3 *Retaining wall (***RW***) problem*

To investigate the effect of *AEV* on the passive earth pressure ($P_P$), a rigid concrete fully frictional wall (δ = $\phi$) of 1 m height (H) and 0.2 m width was modeled with an extension of 0.5 m below the base to prevent restriction of failure mechanisms with the soil bed, shown later in Fig. 7. An aquiclude material was applied to the wall to prevent seepage. Suction was applied by assigning different $H_w$ values from 1 m ($s$ = 0 kPa-fully saturated case) to -4 m below the base ($s$ = 49.05 kPa).

The numerical results for the **RW** case study were validated against an analytical equation proposed by Fredlund and Rahardjo (1993) given below:

$$P_P = \left[\frac{1}{2}k_P\gamma' H^2 + 2c\sqrt{k_P}\,H + 2\,s\,tan\phi^b\sqrt{k_P}\,H \right. \qquad (2)$$

where $k_P$ is the passive lateral earth pressure coefficient, $\gamma'$ is the effective unit weight, $c$ is the cohesion and $\phi^b$ is the internal friction angle with respect to matric suction. A value of $k_P$ = 5.6786 was used for $\phi$ = 30° for the fully frictional wall, according to Antão et al. (2011). The $\phi^b$ value is significantly affected by the applied suction, therefore, in the simulation, different values of $\phi^b$ from 0 to 30° were used, in increments of 2.5°. The results of this series were presented as the normalized passive earth pressure $P_P/(\gamma_d \times H^2)$ and the normalized water table height ($H_w$/H).

The results of the **RW** problem are shown in Fig. 6. At $H_w$/H = 1, corresponding to fully saturated conditions, all response curves converged indicating that *AEV* has no effect on $P_P$ ($s \leq AEV$). As $s$ increased (i.e., when $H_w$/H <1), the curves began to diverge, reflecting the influence of *AEV* on the soil's mechanical response. This illustrated that higher *AEV*s enhance suction retention, therefore significantly affecting $P_P$. For example, at $H_w$/H = -2 and $\phi$ = 30°, an increase of 1.47-fold in $P_P$ was obtained when *AEV* increased from 5 kPa to 20 kPa. This was equivalent to an increase of 4.4° in $\phi$ when modeling the case *AEV* = 5 kPa at the same $H_w$. The peak value of each curve, $P_{P(max)}$, varied with the magnitude of the *AEV* confirming that *AEV* had a significant effect in determining the strength mobilized during passive failure. Beyond the peak, the curves showed a descending trend, indicating a reduction in $P_P$. This reduction was attributed to the gradual desaturation of the soil profile, which diminished $s$ and thus the soil's strength. This post-peak reduction contrasted with the behavior predicted by Eq. 2, where such a decrease is not evident, the predicted $P_P$ values by Eq. 2 increased monotonically. This discrepancy highlighted the necessity of accounting for desaturation effects when modeling the behavior of retaining walls under unsaturated conditions.

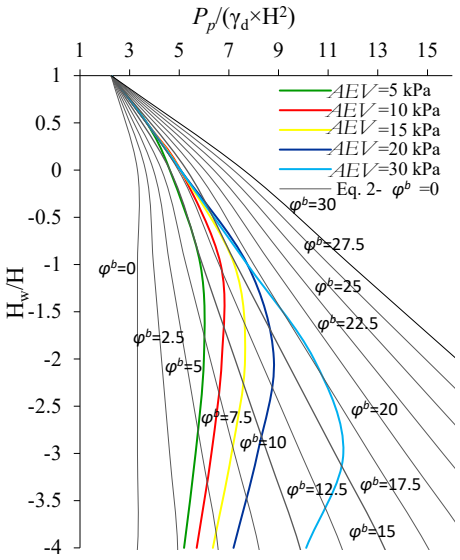


Figure 6. Normalized $P_P$.against normalized $H_w$ for different *AEV*s validated against Eq. 2 (black solid curves) for the **RW** problem for the frictional wall (δ = $\phi$).

Figure 7 displays the failure mechanisms of the modeled scenarios for the **RW** case study at five different *AEV*s values. Additionally, a fully smooth wall condition (δ = 0) was modeled for comparison. The failure modes correspond to the peak $P_P$ shown in Fig. 6, i.e., at $H_w$ = -2 m in all cases, except for the case of *AEV* = 30 kPa where the peak was attained at $H_w$ = -3 m.

The influence of wall friction (δ = $\phi$) was evident when compared to the smooth wall (δ = 0) case. The smooth wall produced only two plane failure surfaces (discontinuities), with a limited horizontal extension of 1.72 m and no failure lines extending beneath the wall base, see Fig.7 (bottom left case). In contrast, the frictional wall (δ = $\phi$) led to wider and more complex failure patterns characterized by multiple discontinuities and failure lines extending clearly beneath the base of the wall. However, comparing the frictional wall cases at various *AEV*s, a significant influence of *AEV* was observed, characterized by wider mobilized failure mechanisms, as shown, for example, in the cases of *AEV* = 5 kPa and *AEV* = 10 kPa in Fig. 7.

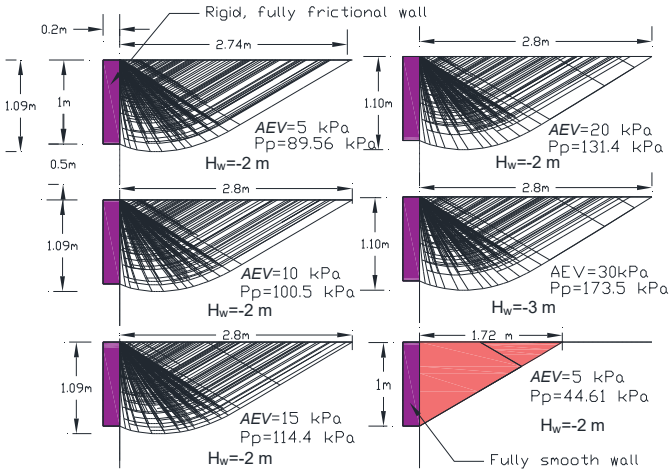


Figure 7. Failure modes for the **RW** problem at various *AEV* values for the frictional wall ($\delta = \phi$) and the smooth wall ($\delta = 0$).

## 2.4 *Tunnel (***TUN***) problem*

The tunnel (**TUN**) case study was analyzed using an axisymmetric model representing half of the tunnel geometry (shown later in Fig. 9). The analysis considered a shallow circular tunnel with a diameter of 2 m, subjected to different $H_w$ and three *AEV*s: 25 kPa, 37.5 kPa, and 50 kPa. The results of the intermediate value of *AEV* = 37.5 kPa represents the average between the lower and higher *AEV*s.

The range of $H_w$ extended from the fully saturated condition ($H_w$ = 15.4 m), where the water table coincides with the ground surface, to –2 m below the origin. The analysis results are expressed in terms of the adequacy factor ($\lambda_F$), defined as the factor by which soil strength should be divided to cause collapse. A $\lambda_F \geq 1$ indicates a stable condition for the tunnel.

Figure 8 shows the results of the **TUN** problem. At full saturation ($H_w$ = 15.4 m), the influence of varying *AEV*s on $\lambda_F$ was minimal, with only slight variations attributed to differences in $\phi$ (30° to 45°). As $H_w$ decreased from full saturation (suction increased), $\lambda_F$ increased significantly, reaching peak stability at $H_w$ = 1 m for all friction angles. This peak indicates an optimal range where suction enhances tunnel stability. Here, the effect of *AEV* became more pronounced, as evidenced by the divergence in $\lambda_F$ among curves with different *AEV*s, particularly at higher $\phi$. Specifically, at $H_w$ = 1 m, increasing *AEV* from 25 to 37.5 kPa and from 25 to 50 kPa resulted in increases in $\lambda_F$ of 4.28% and 11.21%, respectively. These observations highlight the significant role of *AEV* in controlling tunnel stability under varying hydraulic conditions.

Beyond this optimal point, $\lambda_F$ decreased as the soil became increasingly desaturated, with the maximum reduction occurring at $H_w$ = -2 m, where suction's stabilizing effect is essentially decreased. This downward trend suggests that further lowering of $H_w$ would continue to reduce stability, although such cases are not shown in the figure.

Figure 9 illustrates the failure mechanisms obtained for the **TUN** problem at $H_w$ = -2m under different conditions of *AEV* (25, 37.5, and 50 kPa) and two $\phi$ values (30° and 45°). Each subfigure corresponds to a specific combination of these parameters, with the mobilized failure patterns (represented by slip lines and discontinuities) shown accordingly. Since the failure mechanics did not extend below the tunnel's invert, the results are presented only from elevation EL = 7.5 m (below the tunnel invert) to EL = 15.4 m (ground surface).

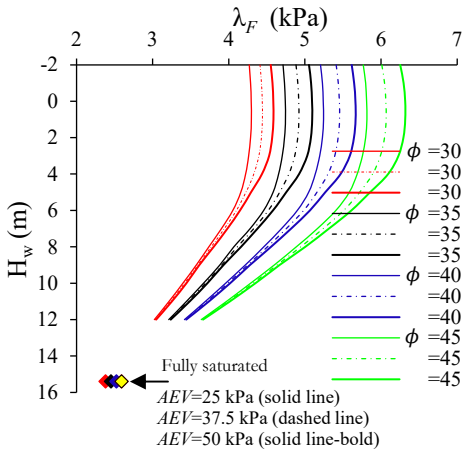


Figure 8. Adequacy factor ($\lambda_F$) versus $H_w$ at various *AEV*s and $\phi$ for the **TUN** problem.

Higher *AEV* values resulted in wider failure mechanisms, see the case at $\phi$ = 45°. However, the most significant observation was within the internal slip zones rather than along the outer failure boundaries. For instance, clear changes in the internal slips can be seen in the $\phi$ = 30° scenarios across all modeled *AEV* values.

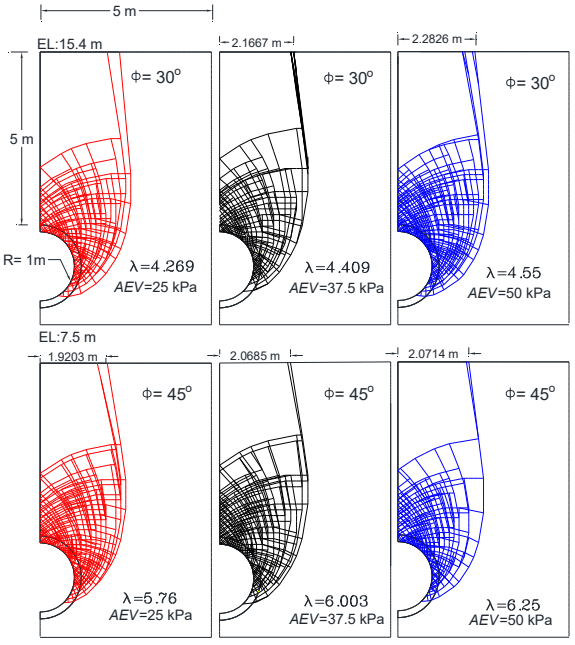


Figure 9. Failure mechanisms for $\phi$ = 30° and 45° at various *AEV*s for the **TUN** problem at $H_w$ = -2m.

## 3 CONCLUSIONS

The air entry value (*AEV*) is a key parameter of the soil-water retention curve, influenced by factors such as pore size and both hydraulic and mechanical hysteresis. While its effect on water retention is well documented in the literature, its influence on the mechanical behavior of soils in geotechnical applications remains less studied.

This study numerically investigated the influence of *AEV* on soil strength in various geotechnical contexts, including bearing capacity (**BC**), slope stability (**SL**), retaining walls (**RW**), and tunnels (**TUN**), using the robust upper bound theorem, **UNSAT-DLO** approach, under different suction profiles. The results, validated against available experimental or analytical solutions (except for the **TUN** problem, which was

not validated due to the lack of experimental data or analytical solutions), demonstrated that increases in *AEV* significantly enhance the mechanical characterization. Based on the results of this study, the following conclusions can be drawn:

1. For the **BC** problem, for example, increase in *AEV* resulted in a significant rise in bearing capacity factor ($N_\gamma$). Increase in *AEV* from 2.3 kPa to 4 kPa at suction ($s$) = 3.796 kPa, at angle of shearing resistance ($\phi$) = 44° resulted in an increase of 1.88 in $N_\gamma$. This was equivalent to an increase of 3.5° in $\phi$ when modeling the case $s$ = 3.796 kPa at *AEV* = 2.3 kPa. Even higher increase in $N_\gamma$ (4.83) at $s$ = 5.58 kPa was observed when *AEV* increased from 2.3 kPa to 6 kPa.

2. For the **SL** problem, increasing *AEV* from 5 to 20 kPa at cohesion (c) = 20 kPa and $\phi$ = 30° resulted in an increase of 1.13 in factor of safety (FS), which was equivalent to an increase of 10° in $\phi$ when modeling the case of *AEV* = 5 kPa at the same cohesion value.

3. Similarly, for the **RW** analysis, higher *AEV* values led to substantial increases in passive earth pressure ($P_P$). An increase of 1.47-fold in $P_P$ was obtained when *AEV* increased from 5 kPa to 20 kPa at a water table height ($H_w$) = -2 and $\phi$ = 30°, which was equivalent to a 4.4° increase in $\phi$ for the case of *AEV* = 5 kPa to achieve the same fold increase as the increase of *AEV*.

4. Finally, for the **TUN** problem, at $s$ = 141.26 kPa, increases of 9.3% and 18.2% in adequacy factor ($\lambda_F$) were obtained when *AEV* increased from 25 to 37.5 kPa and to 50 kPa, respectively.

5. The study also included analyses of the failure patterns at various *AEV*s for all modeled problems. The analyses revealed that wider and/or deeper failure mechanisms were obtained for the higher *AEV*s. To sum up, these findings highlight the importance of considering *AEV* variations in geotechnical design under various drying and wetting conditions (hydraulic hysteresis) and mechanical hysteresis.

## 4 ACKNOWLEDGEMENTS

The author gratefully acknowledges Salahaddin University-Erbil for its support and technical assistance during this research.

## 5 REFERENCES

Antão, A.N., Santana, T.G., Vicente da Silva, M. and da Costa Guerra, N.M., 2011. Passive earth-pressure coefficients by upper-bound numerical limit analysis.. *Canadian Geotechnical Journal,* 48(5), pp. 767-780.

Bell, J.M., 1966. Dimensionless parameters for homogeneous earth *slopes*. *Journal of the Soil Mechanics and Foundations Division,* 92(5), pp. 51-65.

Chiu, C.F., Ni, X.W. and Zhang, L.S., 2014. Effect of hydraulic *hysteresis* on shear strength of unsaturated clay and its prediction using a water retention surface. *Engineering geology,* Volume 173, pp. 66-73.

Fredlund, D.G. and Rahardjo, H., 1993. *Soil Mechanics for Unsaturated Soils.* s.l.:John Wiley & Sons.

Kim, J., Hwang, W. and Kim, Y., 2018. Effects of hysteresis on hydro-mechanical behavior of unsaturated soil. *Engineering Geology,* Volume 245, pp. 1-9.

Lloret-Cabot, M., Wheeler, S. J., Pineda, J. A., Romero, E., & Sheng, D., 2018. From saturated to unsaturated conditions and vice versa. *Acta Geotechnica,* 13(1), pp. 15-37.https://doi.org/10.1007/s11440-017-0577-6.

Lu, N. and Likos, W.J., 2004. Rate of capillary rise in soil.. *Journal of geotechnical and Geoenvironmental engineering,,* 130(6), pp. 646-650.

Nuth, M., & Laloui, L., 2008. Advances in modelling hysteretic water *retention* curve in deformable soils. *Computers and Geotechnics,* 35(6), pp. 835-844.

Pham, H.Q., Fredlund, D.G. and Barbour, S.L., 2003. A practical *hysteresis* model for the soil–water characteristic curve for soils with negligible volume change. *Geotechnique,* 53(2), pp. 293-298.

Romero, E. E., 1999. *Characterisation and thermo-hydro-mechanical behaviour of unsaturated Boom clay: an experimental study.* Barcelona, Spain, Doctoral thesis, Universitat Politècnica de Catalunya.

Shwan, B. J., 2015. *Experimental and numerical study of the shear strength of unsaturated sand,* Doctoral dissertation, University of Sheffield, Sheffield, UK: s.n.

Shwan, B. J., 2017. The effect of soil water retention curve hysteresis on *the* strength of unsaturated soils. *Journal of Duhok University,* pp. 285-292.

Shwan, B. J., 2022. Upper bound analysis of suction effect on tunnel *stability*. *International Journal of Geomechanics,* 22(9), p. 4022158.

Shwan, B. J., 2023a. Hydro-Mechanical Hysteresis Effect-Induced *Bearing* Capacity Variations for Unsaturated Sand. *International Journal of Geomechanics,* 23(7), pp. 04023106.https://doi.org/10.1061/IJGNAI.GMENG-8255.

Shwan, B. J., 2023b. *Effect of Hydro-Mechanical Hysteresis on Active Earth Pressure for Unsaturated Soils..* Athens, Greece, In E3S Web of Conferences EDP Sciences.(Vol. 382, p. 02006)..

Shwan, B. J., 2023c. Suction effect-induced reduction in shotcrete *thickness* in tunnels. *International Journal of Geotechnical Engineering,* 17(3), p. https://doi.org/10.1080/19386362.2023.2241284.

Shwan, B. J., 2023d. Numerical analysis of slopes treated by nano-*materials*. *Journal of the Mechanical Behavior of Materials,* 32(1), pp. 20220227.https://doi.org/10.1515/jmbm-2022-0227.

Shwan, B. J., 2025. Stability of vertical excavation in unsaturated sand. *Modeling Earth Systems and Environment,* 11(3), pp. 1-14.

Tarantino, A. and Tombolato, S., 2005. Coupling of hydraulic and *mechanical* behaviour in unsaturated compacted clay. *Géotechnique,* 55(4), pp. 307-317..

Vanapalli, S. K., Fredlund, D. G., & Pufahl, D. E., 1999. The influence of *soil* structure and stress history on the soil–water characteristics of a compacted till. *Géotechnique,* 49(2), pp. 143-159.